Available online at www.sciencedirect.com

ScienceDirect

Procedia Structural Integrity 8 (2018) 618–627

Structural Integrity Procedia

www.elsevier.com/locate/procedia

AIAS 2017 International Conference on Stress Analysis, AIAS 2017, 6-9 September 2017, Pisa, Italy

Thermo-structural analysis of components in ceramic material

Gianluca Chiappini[a,*], Marco Sasso[a], Tiziano Bellezze[b], Dario Amodio[a]

[a]*Dipartimento DIISM, Facoltà di Ingegneria, Università Politecnica delle Marche, Via Brecce Bianche, 12, 60100 Ancona, Italy*
bDipartimento SIMAU, Facoltà di Ingegneria, Università Politecnica delle Marche, Via Brecce Bianche, 12, 60100 Ancona, Italy.

Abstract

The aim of this paper is the systematic study of thermo-structural behavior of ceramic components, in particular, mixtures of refractory materials with high thermal and mechanical performance. Using 3-point bending tests, the elastic modulus, ultimate stress and elongation was obtained; measured values, also thanks to the use of DIC optical technology, was correlated with the different thickness and specific weight values of the specimens used. In order to characterize the thermal behavior, thermal conductivity and specific heat were measured. The experimentally determined average values of such thermomechanical properties have been used in FEM thermo-mechanical models, developed using target geometries with shapes and sizes typical of manufactured ceramic products. In order to evaluate the goodness and the correctness of the developed models, some specimens having the the same shape of the target geometries used in FEM models have been tested at different load conditions and constraints.

Peer-review under responsibility of the Scientific Committee of AIAS 2017 International Conference on Stress Analysis

Keywords: ceramic material, thermo-structural analysis, three-point bending test, DIC

1. Introduction

The ceramic components industry has developed refractory mixtures with high thermal and mechanical performance; these mixtures are used to produce valuable components that are typically used in tables and professional

* Corresponding author. Tel.: +39 071 2204440; fax: +39 071 2204801.
E-mail address: g.chiappini@univpm.it

2452-3216
Peer-review under responsibility of the Scientific Committee of AIAS 2017 International Conference on Stress Analysis
10.1016/j.prostr.2017.12.061

countertops (e.g. for analysis laboratories). However, their high performance permits more extensive use of these mixtures: considering both the non-negligible value of the realized products and the increasing production demand, it emerges the need to develop systematic procedures for verifying and predicting the behavior of the ceramic products, when they are subjected to several different exercise loads, especially thermal ones. It is common for this class of components to fracture due to intense mechanical stresses, which are induced by differential thermal expansion between adjacent areas of the component. This may be due, for example, to uneven heating/cooling, and may be accentuated or mitigated by the presence of holes, thickness variations and geometric complexities in general.

The aim of this paper is therefore to determine the mechanical and thermal characteristics of these materials through experimental tests carried out on different types of specimens. In addition, the aim is to develop numerical models that will allow to study and optimize the behavior of ceramic objects.

Of course, in the study the stochastic nature of physical quantities of interest was considered, due to both the craftsmanship of the manufacturing processes and the inherent variability of the physical characteristics of the mixtures (due to supply and environmental conditions).

The work is divided into several phases that can be summarized as follows:

1) Determination of mechanical and thermal properties
2) FEM Modeling of interest objects
3) Numerical / experimental verification and correlation

Nomenclature

E	Young's Modulus
σ_r	Ultimate stress
ε	Strain
L	Length of the specimen
b	Width of the specimen
t	Thickness of the specimen
C_p	specific heat
α	thermal expansion coefficient
λ	thermal conductivity

2. Methods

2.1. Three-point Bending Test

In order to determine the mechanical characteristics of the ceramic material, three-point bending tests of various thickness specimens, and various types of superficial glaze, was performed. During tests, carried out with an electro-mechanical testing machine Zwick® Z050, load are measured by a 5 kN load cell whereas displacement and deformation are measured using the DIC optical technique (Fig. 1a).

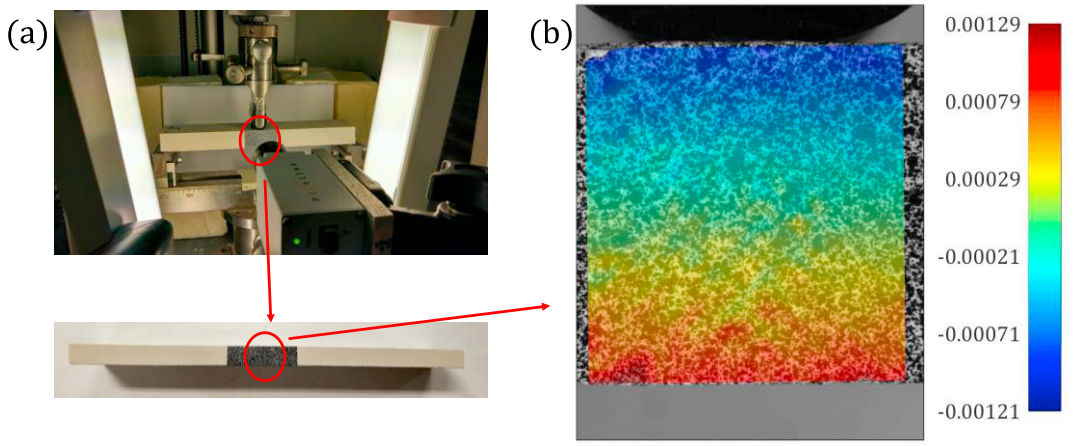

Fig. 1. (a) Experimental setup; (b) map of longitudinal strain.

Images of the speckled area of the specimen are taken using a 1280×1024 resolution CMOS camera, then post processed by a 2D DIC software based on the continuous grid global method [Hild et al., Broggiato et al., Sasso et al.]. The typical accuracy of this technique is about 5/100 of pixel for in-plane displacements [Palmieri et al], which is satisfying for the present application. The strain tensor can be calculated by derivation of displacement field according to Cauchy-Green theory for large displacements [Chung, Amodio et al.], obtaining the full-field distribution maps of each strain component; an example is illustrated in Fig 1b.

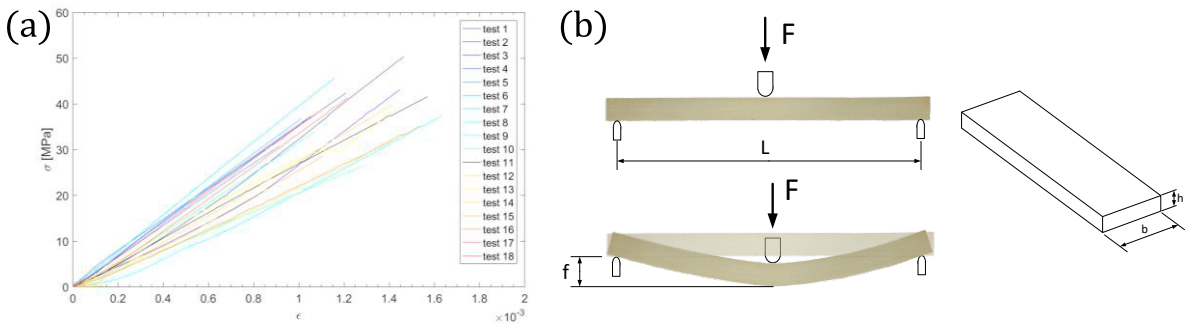

Fig. 2. (a) Experimental Curves σ–ε; (b) Geometric characteristics.

Fig. 2a shows the curves σ–ε obtained from the performed tests: the tension σ and the strain ε are calculated respectively with the formula (1) and (2), where F is the force measured, L, b and h are the geometric dimensions of the specimen as shown in Fig. 2b and f are the displacement calculated with the DIC technique.

$$\sigma = \frac{3FL}{2bh^2} \tag{1}$$

$$\varepsilon = \frac{6fh}{L^2} \tag{1}$$

The curves illustrated in Fig. 2a are very variable, and consequently the mechanical properties measured have a high standard deviation. The mean value obtained with the standard deviation are presented in Table 1, whereas Fig. 3 presents graphically the mean value and the dispersion versus the thickness.

Table 1. Mechanical properties.

	Mean value	Standard deviation
Density [kg/m^3]	2011.04	17.43
Ultimate stress [MPa]	39.70	5.28
Young's Modulus	30.99	5.29

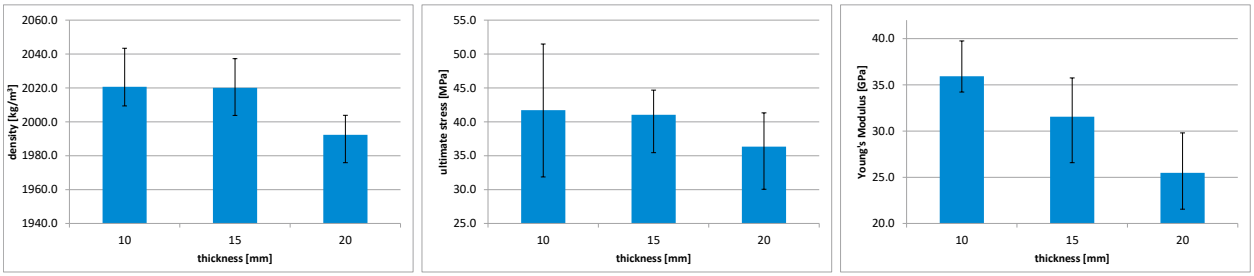

Fig. 3. Mean value with the dispersion of the mechanical properties versus specimen thickness.

The same type of tests have been carried out also on glazed specimens, in order to assess the influence of glaze on the mechanical properties: in particular, the tests was performed with the glazed surface placed alternately up (compression surface) or down (tensile surface) during the bending test. Figure 4 shows the average obtained values, and it can be seen that the glaze has a relevant effect, especially on the ultimate stress.

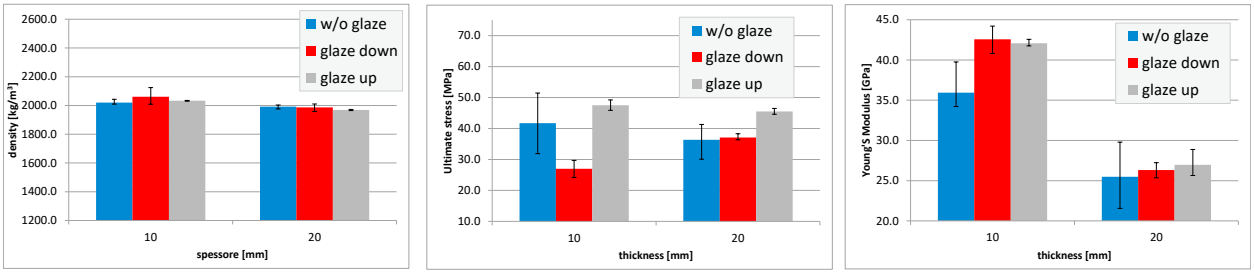

Fig. 4. Mean value and the dispersion for the test on specimen glazed.

Also compression tests was carried out on cylindrical specimens to assess the ultimate compressive stress, whose average value (140 MPa) resulted significantly higher than the tensile one, as expectable for this class of material.

2.2. Determination of specific heat

For determining the specific heat of the samples as a function of temperature, in the range from -20 °C to 100 °C, the procedure described in ASTM E1269-11 standard was adopted [ASTM E1269]. A Seiko® EXSTAR6000 differential scan calorimeter was used to perform all calorimetric measurements (DSC), performing the initial calibration with a synthetic sapphire disk of about 20 mg. Subsequently, for each measurement, 30-35 mg of a sample was weighted and put in an aluminum crucible, which was inserted in the test chamber using an identical empty crucible as reference. The cell was purged by dry nitrogen having a flow rate of 40-45 mL/min during the whole measurement session. The temperature scan rate of 20 °C/min and an initial conditioning time of 4 minutes at -20 °C

was set in the temperature program. After the measurement, the specific heat C_p of each sample was determined as a function of the temperature using the procedure suggested in the above mentioned standard and illustrated in Fig. 5.

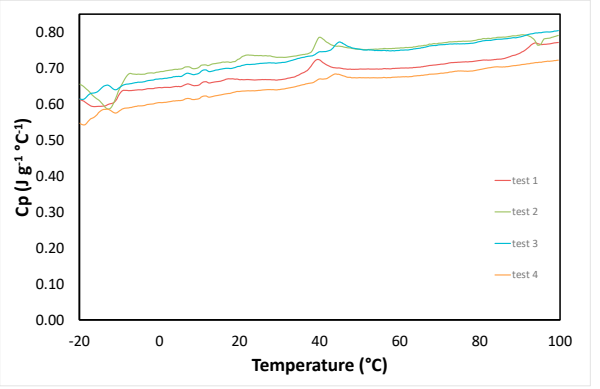

Fig. 5. C_p measured in function of the temperature.

2.3. FEM model

FEM models were developed using the characteristics of the material determined in the experimental tests. The geometry used (Fig. 6a) is a tile of dimensions 300×240 mm, with areas of different thickness and lower ribs connected with the upper surface. The tile was loaded with a 1000 N vertical bending force applied in 4 different points, while the constraint is provided by 3 simple supports as shown in Fig. 6b.

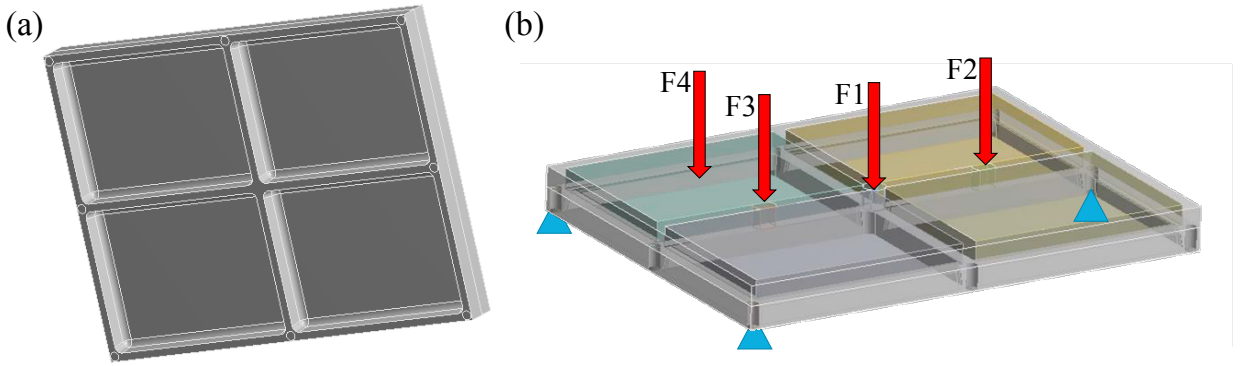

Fig. 6. (a) Geometry model; (b) Load in 4 different positions e 3 support .

The mesh of the model is made up of 254000 nodes and 147000 elements. For each model, the maps of displacement and safety factor, calculated using the Mohr-Coulomb criterion, were obtained. These maps were then compared with the values obtained from experimental tests carried out on tiles of the same geometry.

With the aim of analyzing the structural thermal behavior of a ceramic tile, a thermo-structural model was developed using the same geometry. In the thermal transient model the tile was subjected to a heating and cooling cycle, both lasting 10 minutes. The ambient temperature was considered to be 20 °C. In the heating cycle a 70W thermal power was inserted under one of the four quadrants created by the ribs. The natural air convection was set with a convection coefficient of 10 W/m^{2}K on the entire surface of the tile except for the quadrant where the thermal power was applied. In addition, an emissivity coefficient 0.9 has been considered for the irradiation of the upper and

lateral surfaces. In the cooling cycle, the thermal source was removed from the quadrant, obviously, and a decreased natural convection coefficient was applied.

Fig. 7a shows the temperature distribution at the end of heating, with a maximum peak of 136.8 °C.

The temperature distribution, obtained with the transient thermal model, was used as the thermal load input in a static structural model to perform a thermo-mechanical analysis. The maximum registered equivalent stress is about 18 MPa with a minimum safety factor of about 2.15 (Fig. 7b).

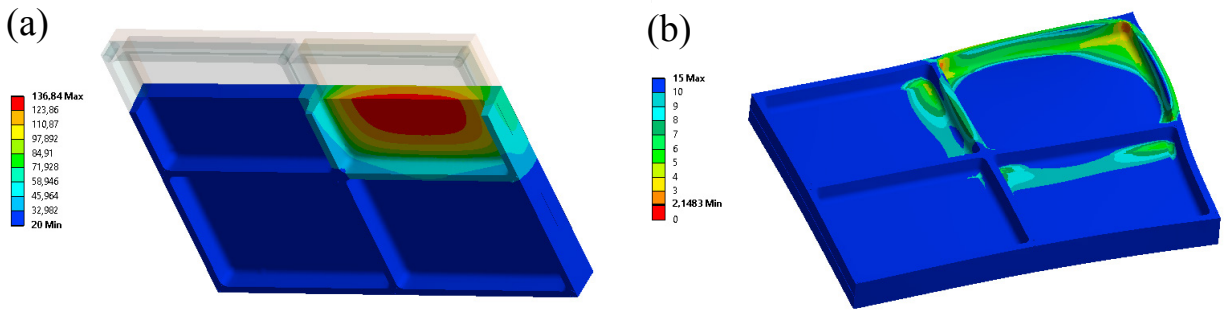

Fig. 7. (a) Temperature map and (b) Safety factor.

2.4. Experimental test on Whole Tiles

In order to evaluate the accuracy of the developed FEM models, experimental bending tests were performed with a tile of the same geometry used in FEM models. Four different tests were carried out with an electro-mechanical testing machine Zwick® Z050, with the force applied at the same points as the FEM models. Fig. 8 shows the experimental setup used. The tests were performed up to the breaking point and load was measured by a 5 kN load cell while the displacement of the tile was measured using the DIC optical technique.

Images of the speckled area of the tiles are taken using 4 CMOS cameras with a 1280×1024 resolution, calibrated in a common global system and then post processed by a 3D DIC software based on the continuous grid global method [Rossi et al.].

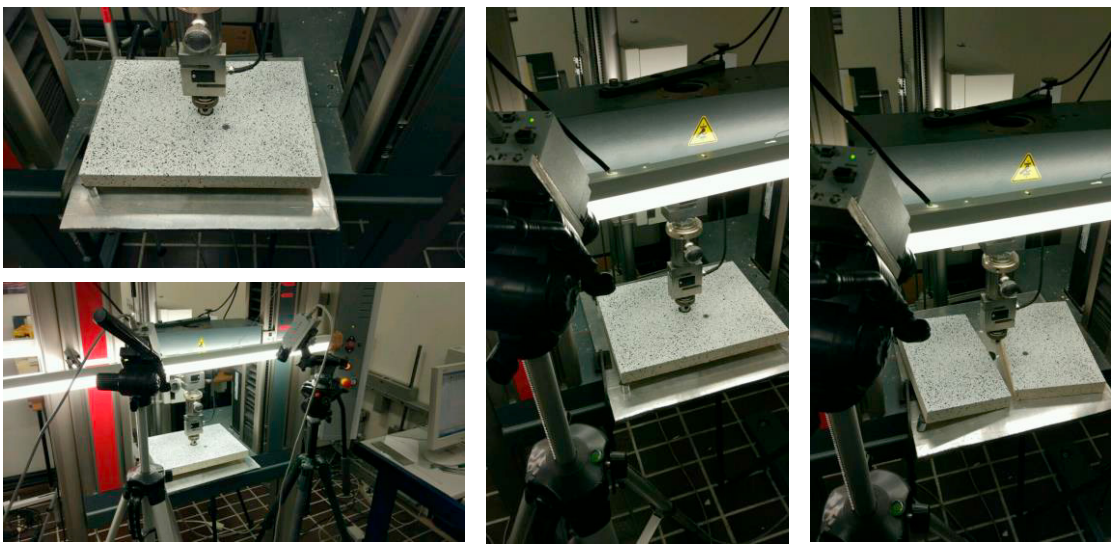

Fig. 8. Experimental setup.

3. Results

Table 2 shows the values of the breaking strength obtained with the 4 FEM models and the experimental tests, whereas Fig. 9 shows the map of the safety factor compared with the breaks obtained in the experimental tests.

Table 2. Force Comparison.

	Experimental	FEM model
Load position F1	1600.90	2000
Load position F2	2608.70	2600
Load position F3	1855.40	2040
Load position F4	1676.10	2800

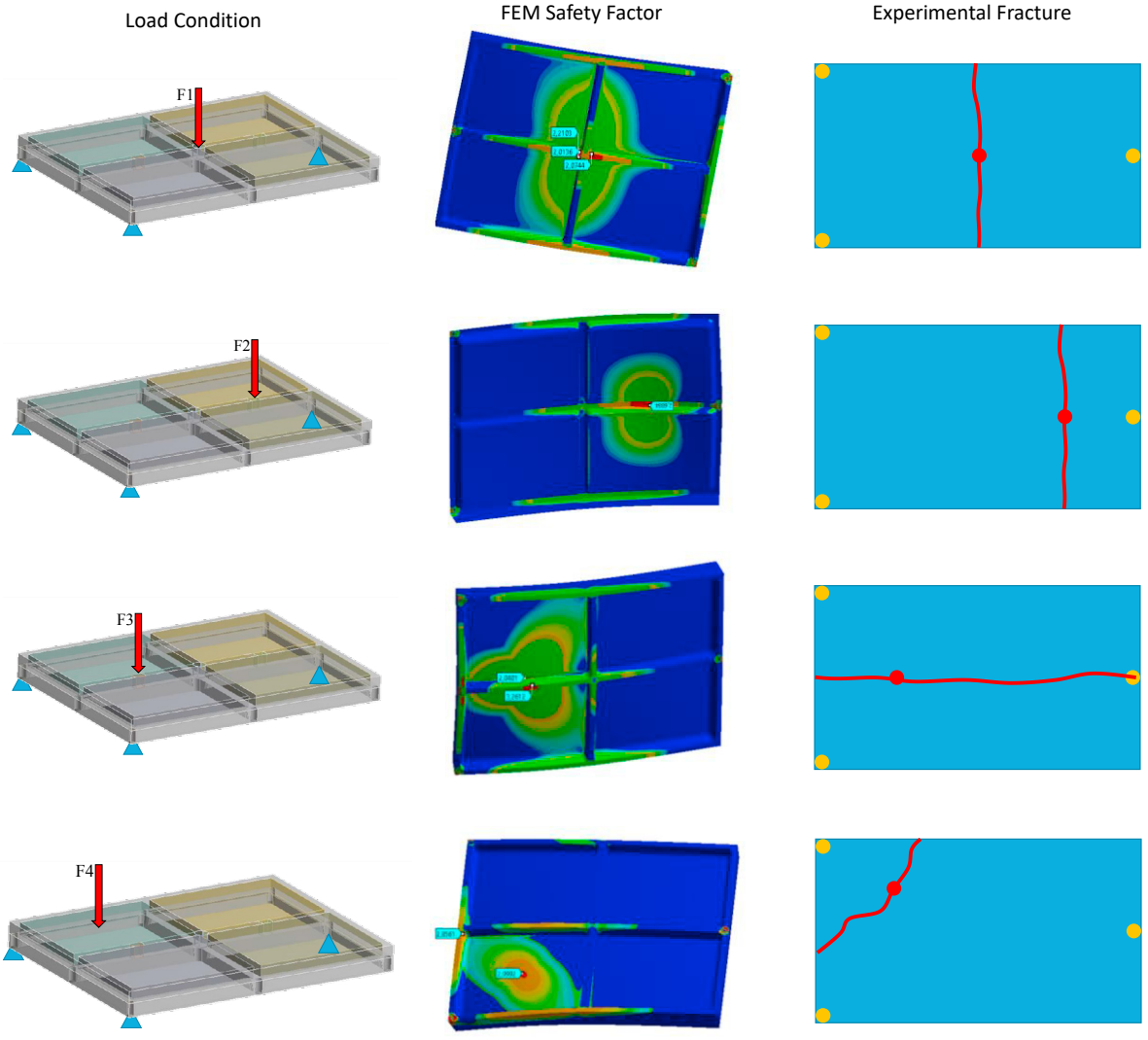

Fig. 9. Confront FEM – sperimentale: coefficient di sicurezza e modi di rottura sperimentali.

The breaking initiation in the experiments occurred where the most critical value of the safety coefficient was achieved. Also the directions of crack opening and propagation are perfectly compatible with the FEM results, in the sense that the opening occurred perpendicular to the direction of predicted maximum tensile stress, and the propagation occurred along the path of minimum safety factors. Indeed, in loading conditions 1 and 2 the breaking occurs in a transverse direction (y) starting at the point of load application, and is due to longitudinal tensile stresses (x). Instead, in the load condition 3 the breaking occurs in the longitudinal direction (x) due to the high stresses in the transverse direction (y) that are present at the plate-rib fillet.

Concerning the load values at failure, there is an optimal correspondence between the numerical and experimental obtained values in cases 2 and 3; also the case 1 had a good prediction (considering the dispersion in the ultimate stress of the material), the slightly higher discrepancy possibly be due to imperfections in the fillets at the four-ribs intersection. With regard to case 4, the failure mode was very well captured, in terms of crack initiation and propagation. The non-negligible difference between predicted and real load to failure could not be further investigated because of the limited number of specimens available at this stage; however it is likely to be due to a local indentation effect of the punch on the flat ceramic surface.

Fig. 10 illustrates the results of the optical processing of the images acquired during the experimental tests: vertical movements (normal to the surface of the tiles) are calculated using three different pairs of stereoscopic cameras.

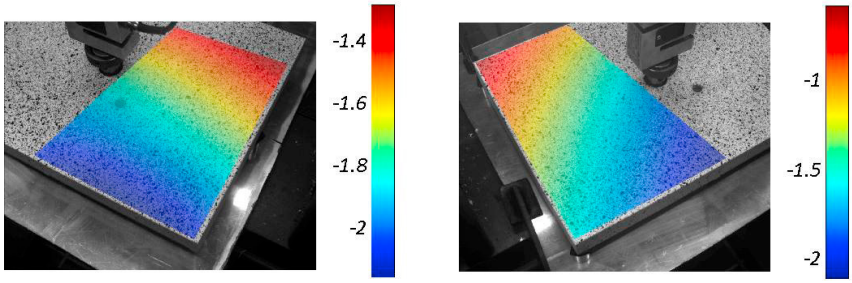

Fig. 10. Displacement maps (in mm) obtained with different pairs of cameras.

Fig. 11a shows the global map of the vertical displacement (z) computed with respect to a global reference system; it has been obtained by combining the individual maps of Figures 10. It is seen that the displacements at the support locations are quite far from being null. This happened because the three supports on which the tiles were mounted were made of rubber disks (to avoid local breaks in the experimental tests). For this reason, the displacements measured at the support locations were used to calculate the ideal plane passing through them, which was then subtracted from the map of Fig. 11a. This procedure allowed to get rid of the rigid roto-traslation and to obtain the final map (Fig. 11b) of the vertical displacement due to deformation only.

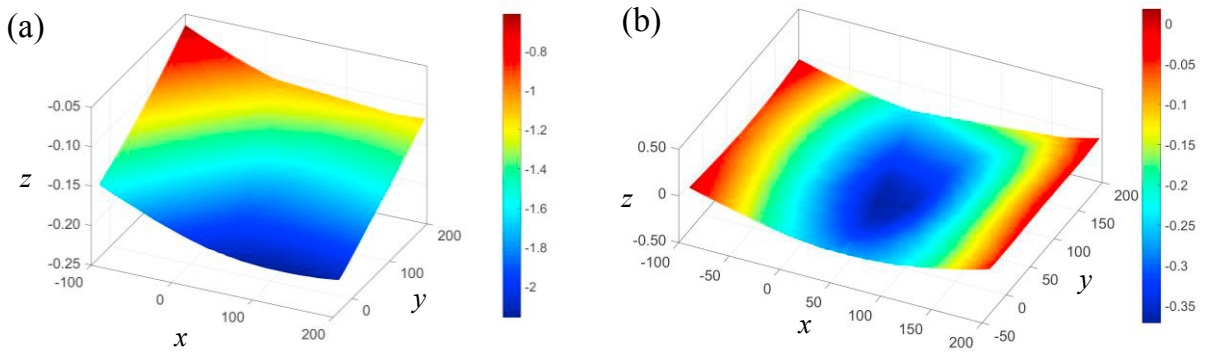

Fig. 11. (a) Global displacement map (b) Final displacement due to deformation only

The measured global displacement was compared to that resulting from the FEM model shown in Figure 12. A force of 1000 N was applied to the FEM model, while the map shows in Fig. 11b was associated with a breaking load of 1600 N. Then, the proportional numeric displacement is 0.201×1600/1000 = 0.32 mm, which is similar to the displacement experimentally measured.

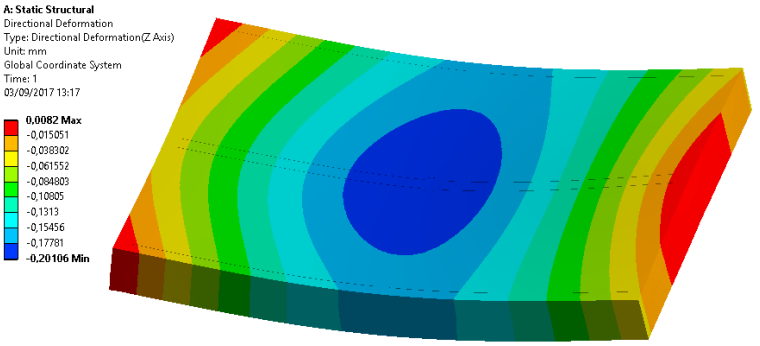

Fig. 12. Displacement FEM with F = 1000 N

4. Discussions

In this paper a mechanical and thermal characterization of a ceramic material was performed. By means of 3-point bending tests on parallelepiped samples, enriched by the use of DIC optical technique, the mechanical properties of the material were obtained. The test results provided a high standard deviation: this is due to the craftsmanship of the processed that are employed for the manufacturing of these tiles. In addition, certain mechanical properties (i.e. ultimate stress and Young's Modulus) present a dependence on the thickness: this is still due to the production process, where the efficiency of the moisture drying phase depends on the thickness of the object.

A FEM model was developed to conduct numerical analyses of ceramic components subjected to both mechanical and thermal loads. Experimental mechanical tests have been conducted on ribbed tiles, whose geometry is comparable to that of commercial products. The comparison between numerical data and experimental results suggested that the FEM model and the adopted failure criterion (i.e. Mohr-Coulomb) are able to predict the behaviour of items made of ceramic material. This can be used by the product developers in order to properly design the future ceramic objects, especially in terms of thickness, fillet radius and ribs geometry, and to improve their thermo-mechanical performances.

Acknowledgements

The authors gratefully acknowledge Laboratorio Pesaro Srl, and especially Ing. Alberto Falasconi, for the support in the specimens preparation and in the results analysis.

References

Amodio, D., Broggiato, G. B. and Salvini, P. (1995) Finite strain analysis by image processing: smoothing techniques. Strain 31, 151–157.

ASTM E1269 - 11 Standard Test Method for Determining Specific Heat Capacity by Differential Scanning Calorimetry

Hild, F. and Roux, S. (2006) Digital image correlation: from displacement measurement to identification of elastic properties - a review. Strain 42, 69–80.

Broggiato, G. B. (2004) Adaptive image correlation technique for full field strain measurement. Proc. of ICEM-12th International Conference on Experimental Mechanics, Bari.

Chung, T. J. (1988) Continuum Mechanics. Prentice Hall International Editions.

Palmieri, G., Chiappini, G., Sasso, M., Papalini, S. Hyperelastic materials characterization by planar tension tests and full-field strain measurement (2009) Society for Experimental Mechanics - SEM Annual Conference 2009, 4, pp. 2232-2238.

Rossi, M., Chiappini, G., Sasso, M. Characterization of aluminum alloys using a 3D full field measurement (2010) Society for Experimental Mechanics - SEM Annual Conference and Exposition on Experimental and Applied Mechanics 2010, 1, pp. 93-99.

Sasso, M., Chiappini, G., Rossi, M., Cortese, L., Mancini, E. Visco-Hyper-Pseudo-Elastic Characterization of a Fluoro-Silicone Rubber (2014) Experimental Mechanics, 54 (3), pp. 315-328.